REPORT DOCUMENTATION PAGE

Form Approved
OMB No. 0704-0188

AD-A272 134

1. AGENCY USE ONLY (*Leave blank*)

2. REPORT DATE
JUNE 1993

3. REPORT TYPE AND DATES COVERED
JOURNAL ARTICLE

4. TITLE AND SUBTITLE
A T_I: AL_2O_3 MASTER-OSCILLATOR/POWER-AMPLIFIER SYSTEM

5. FUNDING NUMBERS
C — F19628-90-C-0002
PE —63217C

6. AUTHOR(S)
K.F.WALL, P.A.SCHULZ, L.AGGARWAL, P.LACOVARA, A.SANCHEZ

7. PERFORMING ORGANIZATION NAME(S) AND ADDRESS(ES)
Lincoln Laboratory, MIT
P.O. Box 73
Lexington, MA 02173-9108

8. PERFORMING ORGANIZATION REPORT NUMBER
JA-6795

9. SPONSORING/MONITORING AGENCY NAME(S) AND ADDRESS(ES)
STRATEGIC DEFENSE INITIATIVE ORGANIZATION
OSD/SDIO/SN
THE PENTAGON
WASHINGTON, DC 20301-7100

10. SPONSORING/MONITORING AGENCY REPORT NUMBER
ESC-TR-93-295

11. SUPPLEMENTARY NOTES
IEEE JOURNAL OF QUANTUM ELECTRONICS, VOL. 29, NO.6, JUNE 1993

12a. DISTRIBUTION/AVAILABILITY STATEMENT
Approved for public release; distribution is unlimited.

12b. DISTRIBUTION CODE

13. ABSTRACT (*Maximum 200 words*)

Abstract—We have constructed a multistage Ti:Al_2O_3 master-oscillator/power-amplifier system which generates 115 ns, 0.38 J pulses at 800 nm. The system is tunable from 760 to 825 nm and has a repetition rate of 10 Hz. Measurements of the output pulse demonstrate near diffraction-limited performance and a Fourier transform-limited bandwidth of ~4 MHz.

14. SUBJECT TERMS
T_I:AL_2O_3 LASER; LASER AMPLIFIER; MOPA
MASTER-OSCILLATOR/POWER-AMPLIFIER SYSTEM

15. NUMBER OF PAGES
10

16. PRICE CODE

17. SECURITY CLASSIFICATION OF REPORT	18. SECURITY CLASSIFICATION OF THIS PAGE	19. SECURITY CLASSIFICATION OF ABSTRACT	20. LIMITATION OF ABSTRACT
Unclassified	Unclassified	Unclassified	

A $Ti:Al_2O_3$ Master-Oscillator/Power-Amplifier System

K. F. Wall, Peter A. Schulz, *Member, IEEE*, R. L. Aggarwal, P. Lacovara, and A. Sanchez

Abstract—**We have constructed a multistage $Ti:Al_2O_3$ master-oscillator/power-amplifier system which generates 115 ns, 0.38 J pulses at 800 nm. The system is tunable from 760 to 825 nm and has a repetition rate of 10 Hz. Measurements of the output pulse demonstrate near diffraction-limited performance and a Fourier transform-limited bandwidth of ~4 MHz.**

INTRODUCTION

NARROW laser bandwidth, high pulse energies, diffraction-limited beam quality, and wide tunability are often desirable and sometimes necessary attributes of a laser source. For example, long-range coherent laser radar applications require all of these parameters. To address these requirements, we have constructed and operated a $Ti:Al_2O_3$ master-oscillator/power-amplifier (MOPA) which produces transform-limited (~4 MHz), 0.38 J, 0.1 μs with near diffraction-limited beam quality and is tunable from 760 to 825 nm.

A unique aspect of our $Ti:Al_2O_3$ MOPA is that the relatively long pulse duration allows a narrow spectral bandwidth. Pulsed $Ti:Al_2O_3$ lasers are usually operated in a Q-switched or gain-switched mode with short pulse durations and concomitantly large spectral bandwidth. Longer pulsed $Ti:Al_2O_3$ lasers can be obtained using long-duration pump sources, but relaxation oscillations prevent the output from being transform limited and the high instantaneous intensities can damage optics. In addition, it is difficult to spectrally shape (e.g., frequency chirp) the output of a high-power pulsed laser oscillator. We have dealt with these issues by building a CW master oscillator followed by a preamplifier and power amplifiers.

In this paper we will describe a $Ti:Al_2O_3$ MOPA design applicable to an agile-beam laser radar transmitter with particular emphasis on the amplifier design and performance. Previous investigations of $Ti:Al_2O_3$ as an amplifier have included small-signal gain [1], [2] and saturation fluence [3], [4] measurements. A single stage $Ti:Al_2O_3$ MOPA was studied by Barnes *et al.* [5] and a multipass $Ti:Al_2O_3$ preamplifier was constructed by

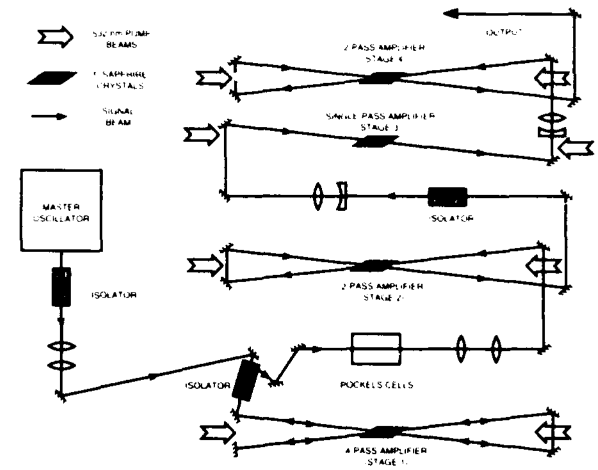

Fig. 1. A schematic of the experimental setup of our $Ti:Al_2O_3$ MOPA. Multipassing of the amplifiers is used extensively to increase the overall gain of the system. The $Ti:Al_2O_3$ amplifier crystals are longitudinally pumped from both sides to increase the gain while minimizing the risk of damage.

Georges *et al.* [6] Regenerative amplification of short pulses in $Ti:Al_2O_3$ has also been studied [6], [7]. In addition, a variety of injection seeded lasers have been investigated as a means of amplifying radiation in $Ti:Al_2O_3$ [8]–[14]. Recently, a multistage $Ti:Al_2O_3$ amplifier was constructed by Sullivan *et al.* [15] which amplified femtosecond pulses to the multiterrawatt level.

In the present paper, a MOPA architecture was chosen because this architecture provides flexibility in choosing pulse lengths and allows one to impose frequency chirps or other forms of frequency modulation on the transmitted radiation. A MOPA, in principle, will preserve the spectral and spatial properties of the master oscillator and allows the generation of long pulses. The above properties are not easily achieved with injection seeding.

The master oscillator of our $Ti:Al_2O_3$ MOPA is a CW, argon-ion laser pumped, single-frequency, $Ti:Al_2O_3$ ring laser [16]. A CW rather than pulsed master oscillator was chosen as it provides the frequency stability required by a laser radar and is consistent with the generation of long pulses. In contrast, a $Ti:Al_2O_3$ Littman laser oscillator constructed by Kangas *et al.* [17] was single frequency but the pulses were only 2 ns long. The master oscillator can be tuned from ~750 to ~850 nm and operates in a TEM_{00} mode. At the peak of the gain profile (~800 nm), the output power is ~0.5 W. A broad-band isolator consisting of a Faraday rotator and a compensating polar-

Manuscript received February 19, 1992; revised September 2, 1992. This work was sponsored by the U.S. Navy for SDIO.
K. F. Wall was with the Lincoln Laboratory, Massachusetts Institute of Technology, Lexington, MA. He is now with Micracor, Acton, MA 01720.
P. A. Schulz, R. L. Aggarwal, and A. Sanchez are with the Lincoln Laboratory.
P. Lacovara was with the Lincoln Laboratory. He is now with Kaman Aerospace Corporation, Tucson, AZ 85706.
IEEE Log Number 9209109.

0018-9197/93$03.00 © 1993 IEEE

ization rotator provides 30 dB of isolation from the Ti : Al_2O_3 amplifier over the tuning range of the master oscillator [18].

The Ti : Al_2O_3 amplifier consists of four longitudinally pumped stages: a four-pass preamplifier, a two-pass amplifier, a single-pass amplifier, and a final two-pass amplifier as shown schematically in Fig. 1. The number of passes through gain regions was optimized using a computer model of the system so as to obtain high gain for the Ti : Al_2O_3 amplifier with good extraction efficiency [19]. The pump lasers for all of the amplifier stages are frequency-doubled Nd : YAG lasers with 10 Hz repetition rates. In what follows we will first describe the pump lasers and the random binary phase plates used to smooth the pump beams. Next, we will discuss the preamplifier and power amplifier stages of the Ti : Al_2O_3 MOPA. Finally the output beam quality, temporal and spectral characteristics, and coherence properties of the Ti : Al_2O_3 MOPA will be described.

Pump Lasers

The pump laser for the preamplifier of the Ti : Al_2O_3 MOPA (stage 1) is a frequency-doubled Q-switched Nd : YAG laser which generates 300-mJ, 532-nm, ~ 10-ns long pulses. The remaining three amplifier stages are pumped with a custom-built Nd : YAG MOPA which is shown schematically in Fig. 2.

The custom Nd : YAG MOPA consists of a master oscillator, an intermediate power amplifier chain, and four parallel chains of power amplifiers. The master oscillator is a Q-switched mode-locked 1064 nm oscillator which produces a train of 100 ps wide mode-locked micropulses separated by 10 ns within an 180 ns envelope (macropulse). (Thus, there are approximately 18 mode-locked pulses within the 180 ns macropulse.) The total energy within a macropulse is ~ 1 mJ. The master oscillator is separated from the first amplifier by an optical isolator to insure the stability of the master oscillator against feedback from reflections, scattering, and amplified spontaneous emission (ASE). Mode locking is used to increase the peak power of the Nd : YAG MOPA by a factor of ~ 100 allowing efficient frequency-doubling with large (~ 1 cm) beam diameters. Large beam diameters are advantageous because large beams have small angular content reducing the angular acceptance requirements of the frequency-doubling crystal. Also, large beams allow a uniform intensity to be maintained over a long distance in the frequency-doubling crystal.

The intermediate power amplifier chain consists of three amplifier heads: the first amplifier has a 6 mm diameter Nd : YAG rod and the following two amplifiers have 9 mm diameter rods. Beam expanders and isolators are used between the amplifiers as depicted in Fig. 2. Depolarization of the signal beam due to stress-induced birefringence within the 9 mm laser rods was reduced from 25 to 5% by the insertion of a 90° polarization rotator between the two amplifiers [20]. The energy per pulse after the intermediate power amplifier is ~ 1 J.

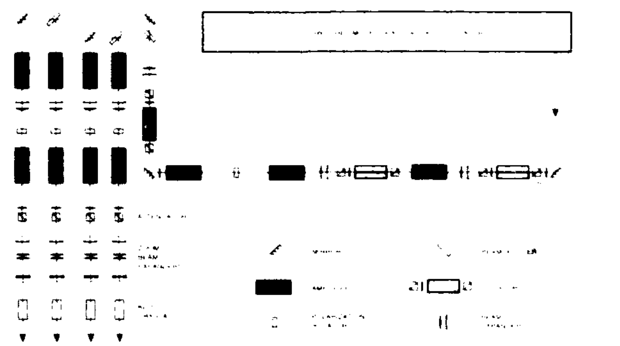

Fig. 2. A schematic of the custom, frequency-doubled, Nd : YAG MOPA used to pump stages 2-4 of the Ti : Al_2O_3 MOPA. The Nd : YAG master oscillator is a Q-switched mode-locked oscillator and is amplified by a chain of three Nd : YAG amplifiers. Next the beam is split equally into four beams and amplified in four parallel amplifier chains. Finally each of the four beams is individually frequency doubled.

The beam next passes through a fourth isolator and is expanded, collimated, and split into four equal beams. These four beams are the inputs to the four parallel chains of power amplifiers. Each amplifier chains consists of a 9 mm amplifier, a 90° polarization rotator, and finally a 12.5 mm amplifier. The output of each power amplifier chain is between 2.5 and 3.0 J. Although the Nd : YAG rod diameters within a power amplifier chain are different, it was still possible to reduce the depolarization from 25% to as little as 5% of the total power using the 90° polarization rotators.

The four output beams from the Nd : YAG MOPA are next sent through variable attenuators each of which consists of a half-wave plate and a polarizer; these attenuators are only used for beam alignment and diagnostic purposes. The 1064 nm beams are then collimated and reduced in size (to ~ 1-cm diameter) by variable magnification beam reducing telescopes before being frequency-doubled to 532 nm. The frequency-doubling is accomplished in parallel using four 25 mm KD*P doubling crystals using Type II phase matching. Doubling efficiencies as high as 38% could be achieved but ~ 30% is routine. The doubling efficiency is not limited by intensity but rather by the beam quality of the Nd : YAG MOPA output. A dichroic mirror is used to eliminate the residual 1064 nm radiation from the 532 nm pump beams.

Random Binary Phase Plates

It was found that the 532 nm pump beams generated by the frequency-doubling crystals damaged the Ti : Al_2O_3 amplifier crystals at spatially averaged pump fluences as low as 3 J/cm^2 due to the presence of high intensity regions (or "hot spots") within the beam profile. These hot spots were the results of intensity modulations on the 1064 nm fundamental beams which consequently produced intensity variations on the 532 nm pump beams. In addition to damage, the spatial variations present in the pump beam profiles were responsible for poor Ti : Al_2O_3 beam quality and for reduced energy extraction efficiency.

In order to solve these problems we use transmissive

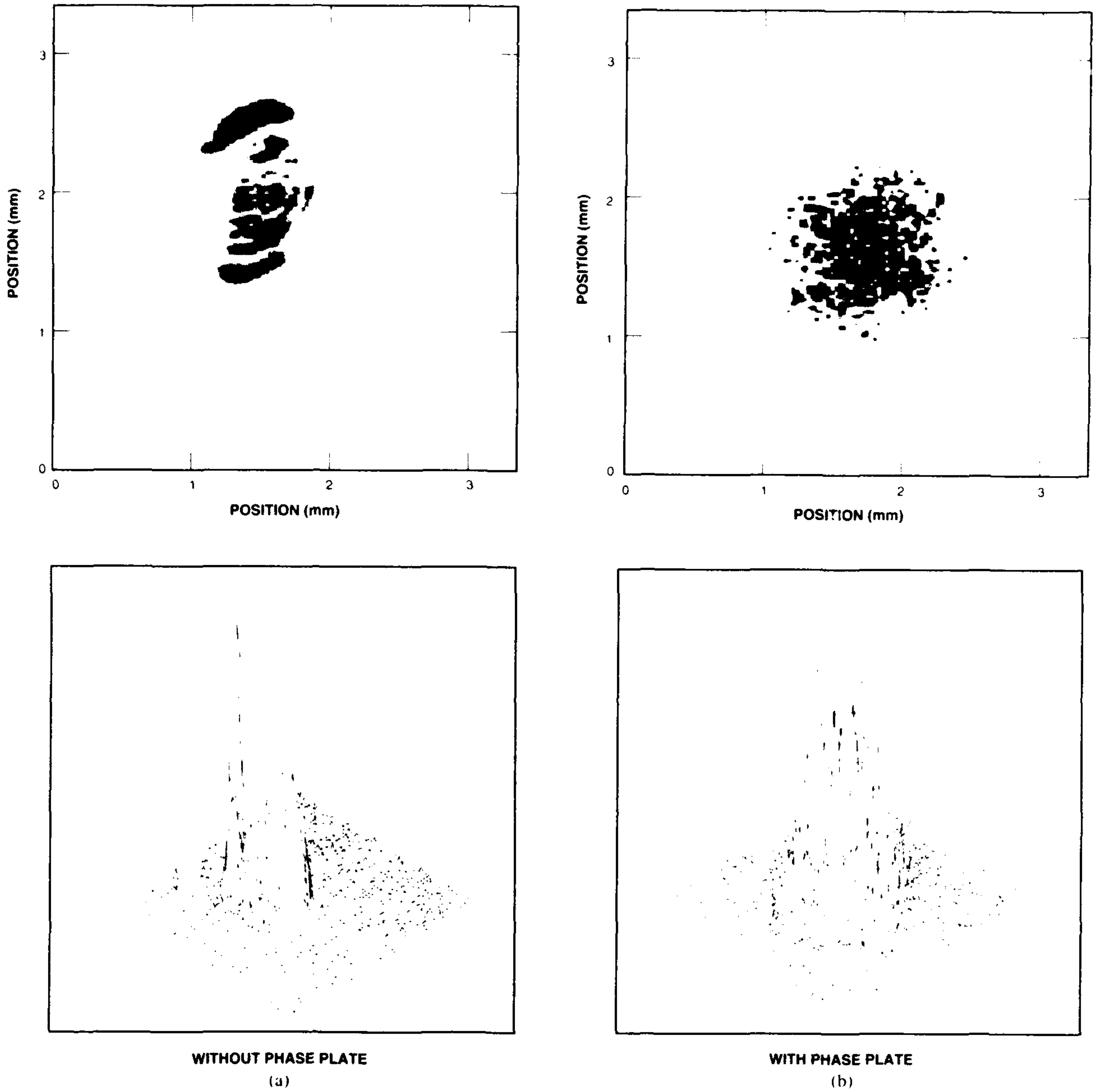

Fig. 3. The effects of beam smoothing using random binary phase plates. (a) shows a density plot (where darker shading represents higher intensity) and a 3-D plot of the intensity profile of a 532 nm pump beam prior to the RBPP. (b) shows the same laser beam after passage through a RBPP and at the focus of a 20 cm focal length lens.

random binary phase plate (RBPP) to smooth the intensity profiles of the 532 nm pump beams [21]. A RBPP consists of a 2-D array of elements where each element introduces a phase shift randomly chosen to be either ϕ_0 or $\phi_0 + 180°$, where ϕ_0 is an arbitrary constant. Such RBPP's have been used in laser fusion experiments to obtain uniform illumination of fusion targets [22]. Other possible designs for RBPP's also exist such as using elements which vary in size or shape (but still tile the surface of the phase plate) or consist of multiple level structures (where, for example, the elements produce net phase differences of 0, 90, 180, and 270°).

For ease of fabrication, we chose the elements of the RBPP to be squares. The size of the square elements was chosen so that the squares were small compared with the scale of intensity variations in the incident laser beam. A relative phase shift of 180° was achieved by precisely etching a transparent substrate using photolithographic techniques. The etch depth d_{etch} required to generate a relative phase shift of 180° for a normal incidence is given by

$$d_{\text{etch}} = \frac{\lambda}{2(n-1)} \tag{1}$$

where λ is the wavelength of the incident laser beam and n is the index of refraction. Small variations in the wavelength or etch depth can be accommodated by tilting the RBPP through an angle θ from the normal. A general-

ization of (1) for arbitrary angles of incidence is

$$d_{\text{etch}} = \frac{\lambda}{2\left\{ n \cos \left| \sin^{-1}\left(\frac{\sin \theta}{n}\right) \right| - \cos \theta \right\}}. \quad (2)$$

The far-field pattern that results after transmission of a laser beam through a RBPP consists of large intensity variations over small spatial scales (speckle) which modulate a smooth envelope given by the Fraunhofer diffraction pattern of a single square aperture. To a good degree of approximation, the central maximum of the Fraunhofer diffraction pattern of a square aperture is cylindrically symmetric.

If a lens of focal length f is used to image the far-field intensity distribution within a $Ti:Al_2O_3$ amplifier crystal the diameter D of the central intensity maximum is approximately given by

$$D \sim \frac{f\lambda}{a} \quad (3)$$

where a is the size of the square elements etched into the phase plate. The diameter d of an individual speckle is approximately

$$d \sim \frac{f\lambda}{\mathfrak{D}} \quad (4)$$

where $\mathfrak{D}$ is characteristic of the diameter of the laser beam incident upon the RBPP. The approximate number of speckles within the central maximum at the focal plane of the lens is $\sim (D/d)^2$ and using (3) and (4) this can be expressed as $(\mathfrak{D}/a)^2$. For an incident beam diameter of 1 cm and a RBPP with 100 μm square elements, there are approximately 10^4 speckles within the central maximum.

Fig. 3 illustrates the smoothing of a 532 nm pump beam using a RBPP with 100 μm square elements. The upper portion of Fig. 3(a) shows a density plot of the intensity profile of a pump beam prior to the RBPP (where darker shading represents higher intensity) in which a hot spot is evident. The lower portion of Fig. 3(a) is a 3-D plot of the same data; the intensity of the hot spot can be seen to be 2 to 3 times more intense than the average intensity. Fig. 3(b) shows the same laser beam after transmission through the RBPP and at the focus of a 20 cm focal length lens. The large scale spatial variations apparent in Fig. 3(a) are removed by the RBPP at the expense of introducing speckle, the small scale spatial variations shown in Fig. 3(b).

One disadvantage of using RBPP's is that only ~80% of the incident energy is present in the central maximum of the far-field pattern. The remainder of the energy appears in the higher diffraction orders. Also, the intensity in a given speckle can be several times larger than the average intensity at the location of the speckle leading to optical damage of the $Ti:Al_2O_3$ amplifier crystals.

The spatial variation of the speckle is not a difficulty as proper choice of pump and signal beam geometries allows the speckle to be averaged out. Averaging of the speckle is achieved by pumping each crystal with two pump beams each of which is smoothed by its own RBPP. Propagation of the signal beam at an angle to the pump beams and multipassing of the $Ti:Al_2O_3$ amplifier crystals provides further averaging. RBPP's are used to smooth all of the 532 nm pump beams in our experiments and as a result, the pump fluence could be increased by a factor of ~2 due to the elimination of hot spots. This made a large difference for the unsaturated stages of the $Ti:Al_2O_3$ MOPA.

$Ti:Al_2O_3$ Amplifiers

Each amplifier stage consists of a $Ti:Al_2O_3$ crystal cut at Brewster's angle to minimize reflection losses. The signal and pump beams propagate in a near collinear (~1°) manner and are both polarized along the c axis of the crystal (π polarization) to maximize the gain and absorption, respectively. The length of each crystal was chosen so that >95% of the pump beam energy is absorbed. Each stage is pumped using RBPP's and each $Ti:Al_2O_3$ crystal is pumped from both sides to maximize the energy absorbed while avoiding damage. The pump beams for stages 1-3 are each split into two equal beams using a beamsplitter and are independently focused on opposite sides of each crystal using separate RBPP's and lenses as shown schematically in Fig. 4. Stage 4 is pumped in a similar manner with the exception that no beamsplitter is necessary since two output beams from the frequency-doubled Nd:YAG MOPA are used to pump this stage.

The first amplifier stage of the $Ti:Al_2O_3$ amplifier is a four-pass preamplifier and is shown schematically in the lower portion of Fig. 1. RBPP's with 150 μm square elements and 40 cm focal length lenses are used to produce a 2 mm pump beam diameter at the face of the $Ti:Al_2O_3$ crystal. The signal beam from the master oscillator is coupled into the preamplifier using a broadband isolator and makes two passes through the $Ti:Al_2O_3$ amplifier crystal. At the completion of the second pass, the beam is reflected from a 1 m focal length mirror back onto itself making two more passes through the $Ti:Al_2O_3$ crystal. After the fourth pass, the beam reenters the broad-band isolator and is rejected by the isolator; this provides the output coupling from the $Ti:Al_2O_3$ preamplifier. The average diameter of the signal beam in this stage is 1.5 mm. The signal beam diameter is smaller than the pump beam diameter and the crossing angle of the pump and signal beams is small to maximize the spatial overlap of the pump and signal beams. Without the RBPP's in this high gain preamplifier, amplification occurred primarily at the hot spots in the pump profile and was sensitive to small thermal and mechanical changes in the system leading to large variations from shot to shot.

Lensing induced in the $Ti:Al_2O_3$ amplifier crystals during pumping, due to both thermal [23] and population induced [24] refractive index changes, made it desirable for the signal beam to pass through the center of the $Ti:Al_2O_3$ crystals on each pass. By passing the signal beam through

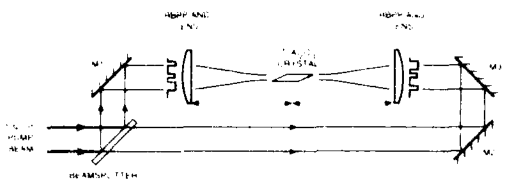

Fig. 4. The pump beam geometry. The beams for stages 1–3 are split into two beams using a beamsplitter and are independently focused on opposite sides of each crystal using separate RBPP's and lenses. M1–M3 are mirrors and f is the focal length of the lens. Stage 4 is pumped in a similar manner with the exception that no beamsplitter is necessary since two output beams from the frequency-doubled Nd : YAG MOPA are used to pump this stage.

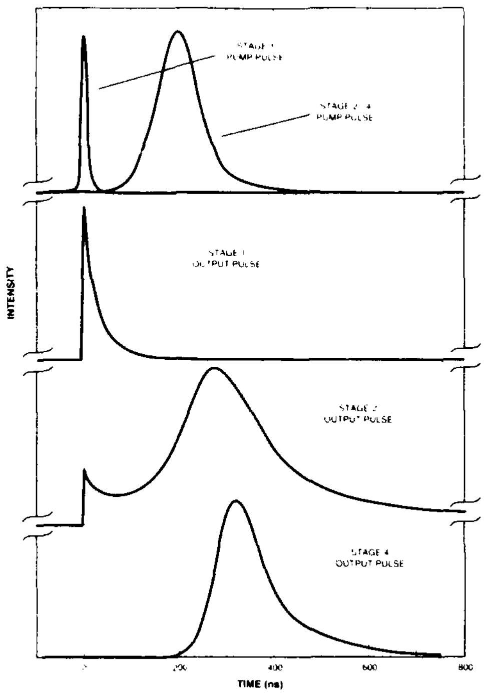

Fig. 5. A timing diagram of the Ti : Al_2O_3 MOPA. The upper portion of the figure shows the temporal profiles of the 532 nm pump pulses. The 800 nm output pulses from stages 1, 2, and 4 are shown below. The pump pulses for stages 2–4 are delayed with respect to stage 1 in order to lengthen the Ti : Al_2O_3 MOPA output pulse.

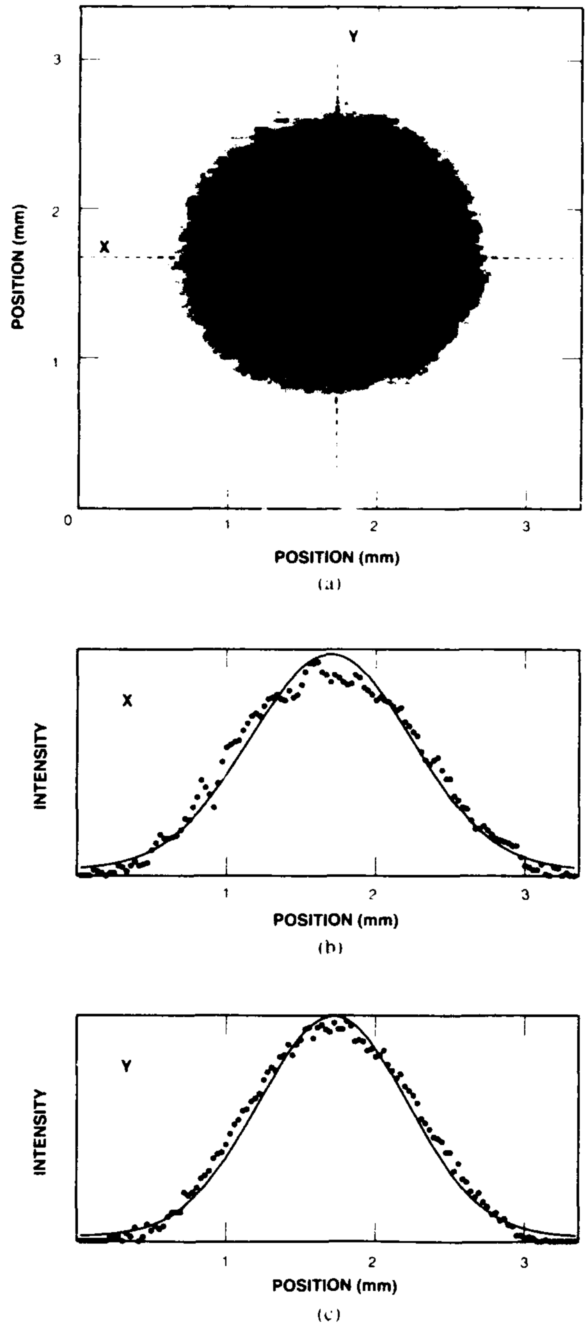

Fig. 6. The beam profile of the preamplifier output. (a) is a density plot (where darker shading represents higher intensity) of the beam profile. (b) and (c) are cross sections of the beam profile through the centroid of the intensity distribution along lines parallel to the x and y axes. The solid lines are fits of Gaussian intensity profiles to the data (solid circles).

the center of the pump-induced lens, the alignment of the signal beam through subsequent stages of the amplifier does not change when the Ti : Al_2O_3 crystals are pumped. The broad-band isolator provides a simple method of passing the signal beam through the pump-induced lens in the preamplifier stage.

As stated earlier, the preamplifier stage is pumped with a Q-switched frequency-doubled Nd : YAG laser. At 800 nm we obtain 4–6 mJ output pulses from the preamplifier when pumped with 225 mJ (incident on the Ti : Al_2O_3 amplifier crystal) and an input signal beam power of 180 mW from the master oscillator. The four-pass gain is 2–3 × 10^5 or a gain of approximately 22 per pass. The output pulse duration is ~100 ns and the temporal profile is shown in Fig. 5. The average power of the CW signal beam from the master oscillator after being transmitted through the preamplifier when not pumped is greater than the average power of amplified signal beam. A pair of Pockels cells are used to pass only the amplified signal beam.

Fig. 6(a) shows a density plot of the signal beam spatial profile at the output of the preamplifier. This profile was taken after the Pockels cells and at a distance which corresponds to the input to the second amplifier stage. Fig. 6(b) and (c) show the fit (solid lines) of Gaussian intensity profiles to cross sections of the data (solid circles) taken through the centroid of the intensity profile along lines parallel to the x and y axes. From the fits it is apparent

TABLE I

Stage	Incident Energy (mJ)	RBPP Element Dimensions (μm)	Focal Length of Lens (cm)	Pump Beam Diameter ($1/e^2$) at Crystal (mm)
1	115	150 × 150	40	2.0
2	190	100 × 100	40	3.0
3	340	75 × 75	40	4.0
4	525	75 × 75	50	5.0

that the signal beam is Gaussian even after being amplified by 10^5.

The power amplifier portion of the $Ti:Al_2O_3$ amplifier system consists of the last three amplifier stages. The frequency-doubled Nd:YAG MOPA provides the pump beams for these stages. The peak of the pump macropulse for stages 2–4 is delayed with respect to the pump pulse for stage 1 by ~ 200 ns (see Fig. 5). This lengthens the output pulse of the $Ti:Al_2O_3$ MOPA by providing a signal input to the last three amplifiers which decreases in time as the gain in these stages is increasing in time. The product of the signal input and gain of the last three stages is, therefore, a flatter function of time yielding longer output pulses. The temporal profile of the output pulse from stage 2, shown in Fig. 5, illustrates the result of the delayed pump pulses. The pulse shape is determined by the input from stage 1, which has decayed substantially but is still finite when stage 2 is pumped, and the high gain of stage 2. Broadband isolators are positioned between stages 1 and 2, and also between stages 2 and 3. Beam expanding telescopes between stages match the signal beam diameters to the pump beam diameters.

Table I lists the pump energy for each stage, the RBPP element dimensions, the focal length of the lens used to image the far field at the $Ti:Al_2O_3$ amplifier crystals, the pump beam diameter ($1/e^2$) at the $Ti:Al_2O_3$ crystals. The value of the energy listed in Table I is the energy incident on each crystal face; the total energy that each crystal is pumped with is twice the listed value since each $Ti:Al_2O_3$ amplifier crystal is pumped from both sides. Successive amplifier stages are pumped with greater amounts of energy. In order not to damage the $Ti:Al_2O_3$ crystals with the pump beams, the pump beam diameters are increased with successive stages and the average fluence is kept constant at ~ 1.3 J/cm^2 (except for the first amplifier stage which is ~ 1.8 J/cm^2). Typical signal beam energies out of stages 2–4 are 10–20, 40–80, and 300–350 mJ, respectively.

The signal beam fluence in the last amplifier stage reached the saturation fluence of $Ti:Al_2O_3$ (~ 1J/cm^2). This was demonstrated by measuring the output pulse energy of stage 4 at 800 nm as a function of the 532 nm pump energy into this stage (with constant pump energy into stages 1 to 3) as shown in Fig. 7. At a pump energy of ~ 300 mJ, the data (solid circles) become linear indicating saturation and power extraction. The slope efficiency calculated by fitting a straight line to the data above

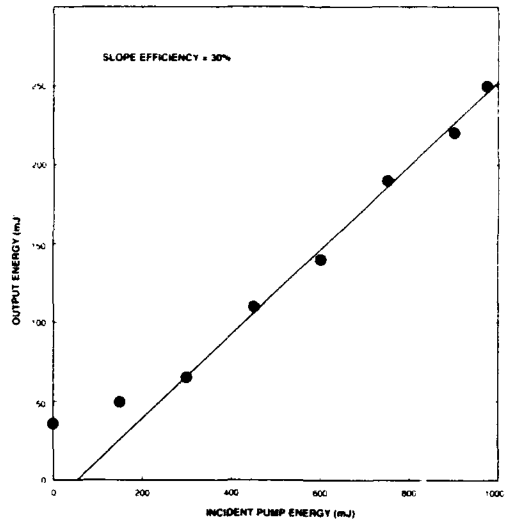

Fig. 7. The output of stage 4 of the $Ti:Al_2O_3$ MOPA at 800 nm. The output energy per pulse was measured as a function of the 532 nm pump energy into stage 4 (with constant pump energy into stages 1 to 3). The curve becomes linear at a pump power of ~ 300 mJ indicating saturation and power extraction. The slope efficiency calculated from the linear portion of the curve is 30% and agrees well with a computer model of $Ti:Al_2O_3$ MOPA.

300 mJ is 30% which is approximately half the limit imposed by the quantum defect. The measured slope efficiency compares favorably with a detailed computer model of our system which takes into account temporal and spatial variations of the pump and signal beams [19].

Optical damage to the $Ti:Al_2O_3$ amplifier crystals by the 532 nm pump beams was encountered in some of our early experiments. It was found that the energies and pump beam diameters listed in Table I could be used safely without optical damage occurring. Since the pump beam profiles are not "flat-topped," the peak fluences that the $Ti:Al_2O_3$ amplifier crystals are exposed to at the center of the spatial profile are greater than the average fluences given above. We estimate that the peak fluence in the first amplifier stage is ~ 9 J/cm^2 and ~ 6.5 J/cm^2 for the three other amplifier stages if we ignore the presence of speckle. In principle, the presence of speckle can increase our estimate by a factor of ~ 2–3. It is also of interest to estimate the peak intensities (at the center of the spatial distribution) that the $Ti:Al_2O_3$ amplifier crystals are subjected to. For the first stage we estimate the peak pump beam intensity to be ~ 1 GW/cm^2 and for the remaining three stages the peak pump beam intensity is ~ 5

GW/cm^2 again ignoring the presence of speckle. When damage occurred, it typically took the form of needle-like damage tracks in the bulk of the crystal.

Output Beam Quality

Several of the $Ti:Al_2O_3$ amplifier stages are multi-passed to increase the signal gain and the overall signal gain of the system was $\sim 2 \times 10^7$. Significant aberration of the signal beam was possible due to the large number of passes through gain regions (nine), mirrors reflections (twenty-eight), and transmission through surfaces (ninety-four). The near- and far-field properties of the output beam were investigated in order to quantify these effects.

Fig. 8(a) shows a density plot of a typical near field beam profile ~2 m from the output of the $Ti:Al_2O_3$ MOPA system at 800 nm corresponding to an output energy per pulse of 340 mJ. The 2 m distance insured that the measurement of the beam profile and output energy were not affected by ASE. Cross sections through the centroid of the data are shown in Figs. 8(b) and 8(c). The fit of Gaussian intensity profiles to the data show that the beam can be characterized as elliptically Gaussian with an aspect ratio of 1.3. The ellipticity originates from the use of Brewster angle faces on the $Ti:Al_2O_3$ crystals. The beam profile measurements also show that the signal beam is not noticeably affected by the speckle which is present in the pump beams (due to the RBPP's).

The far-field properties of the $Ti:Al_2O_3$ MOPA output were determined by examining the intensity distribution at the focus of a 1-m focal length lens as shown in Fig. 9. The intensity profile is again an elliptical Gaussian but, as expected, the major and minor axes of the ellipse are reversed from those shown in Fig. 8. In order to rule out the possibility that a broad low intensity "pedestal" (undetected by the beam profile measurement) was not present in the far field, the far-field properties of the output beam were determined by measuring the transmission of the focused output beam through a circular aperture. The aperture was positioned at the focus of a 1 m lens and centered by maximizing the transmission. Assuming that the beam waist at the focus of the lens had a circularly symmetric Gaussian profile, the $1/e^2$ beam diameter of the intensity d is given by

$$d = 2r \sqrt{\frac{2}{\ln [P_0/(P_0 - P_t)]}} \tag{5}$$

where P_t is the power transmitted through the pinhole, P_0 is the incident power, and r is the radius of the pinhole. Using this method we obtained a value of $d = 400 \pm 20$ μm. Assuming a collimated Gaussian beam of $1/e^2$ diameter $\mathfrak{D}$ incident upon the lens, the diffraction-limited $1/e^2$ beam diameter of the intensity D_{dl} at the focus of a lens is given by

$$D_{dl} = \frac{4}{\pi} \frac{f\lambda}{\mathfrak{D}} \tag{6}$$

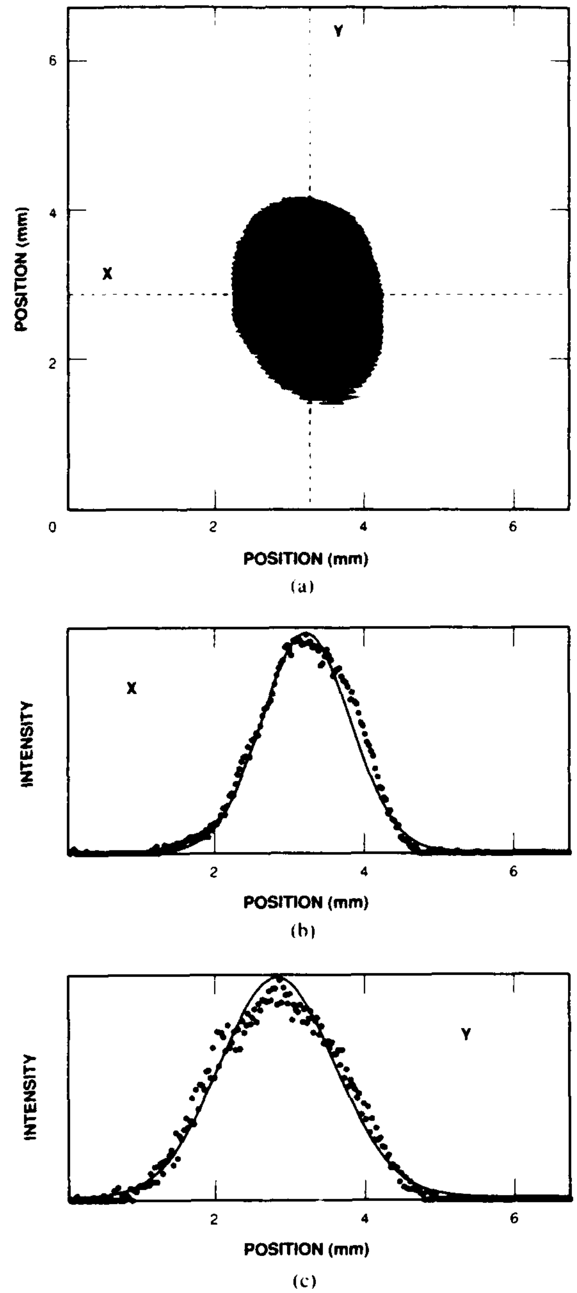

Fig. 8. The near-field profile of the $Ti:Al_2O_3$ MOPA output beam. (a) is a density plot (where darker shading represents higher intensity). Profiles through the centroid of the data along lines parallel to the x and y directions are shown in (b) and (c) where the data are indicated by the solid circles and the solid lines are Gaussian fits to the data.

where f is the focal length of the lens. For $f = 1$ m, $\lambda = 800$ nm, and $\mathfrak{D} = 2.7$ mm (the average of the x and y $1/e^2$ beam diameters obtained from Fig. 8), the calculated value of D_{dl} is 375 μm. The ratio of the measured beam diameter d to the theoretical diameter D_{dl} is 1.1 and we conclude that the output of the $Ti:Al_2O_3$ MOPA is near diffraction limited. It should be noted that the data shown in Fig. 9 yields a beam diameter of less than 400 μm (in fact, less than D_{dl}). We attribute this difference to systematic and statistical errors in our beam profile measurements.

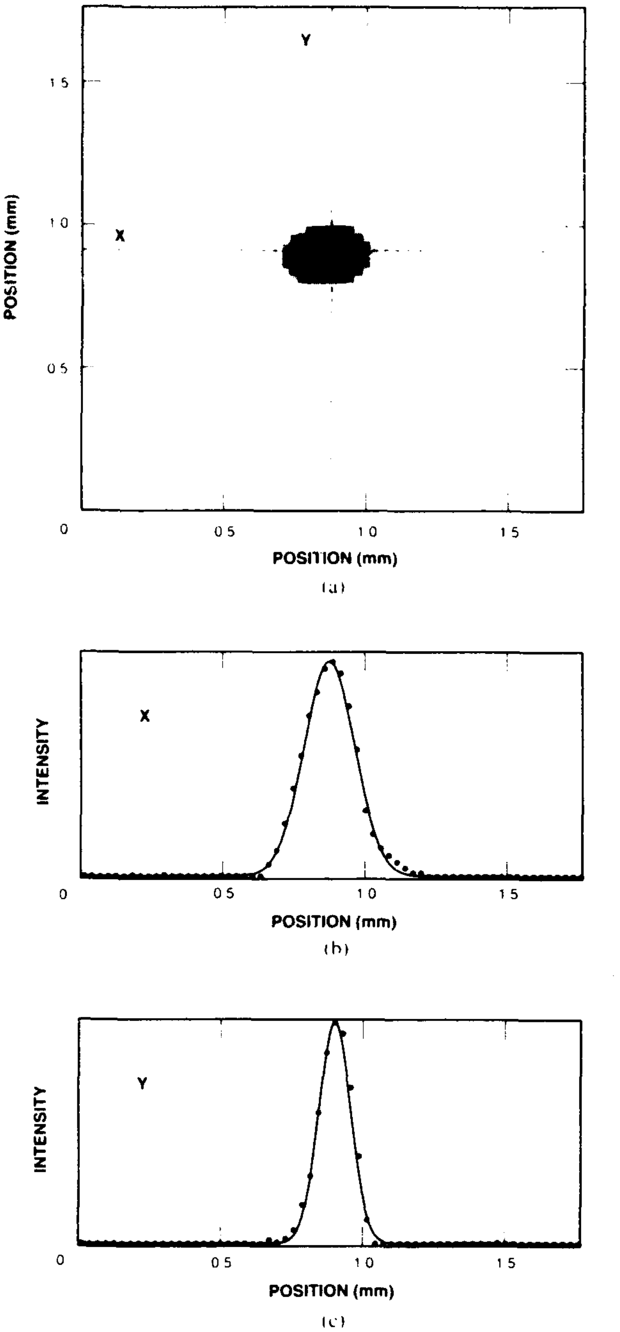

Fig. 9. The far-field profile of the Ti:Al_2O_3 MOPA output beam. (a) is a density plot (where darker shading represents higher intensity). Profiles through the centroid of the data along lines parallel to the x and y directions are shown in (b) and (c) where the data are indicated by the solid circles and the solid lines are Gaussian fits to the data. The far field profile was obtained by focusing the output of the Ti:Al_2O_3 MOPA with a 1 m focal length lens.

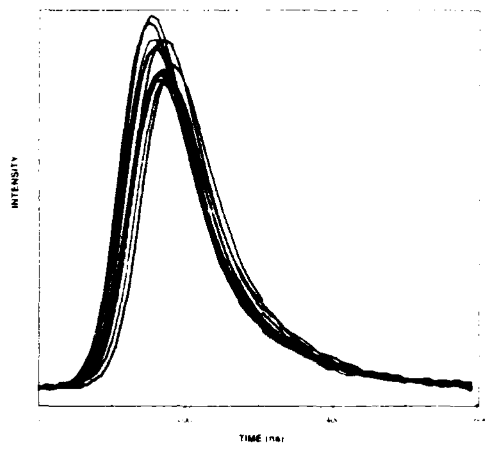

Fig. 10. The shot to shot variation of the Ti:Al_2O_3 MOPA output shown for fifteen consecutive pulses. The width of an individual pulse is 115 ns FWHM and the pulse-to-pulse amplitude variation is < 10%. The temporal jitter is ~20 ns and the pulses are smooth and show no structure on times as small as 20 ns.

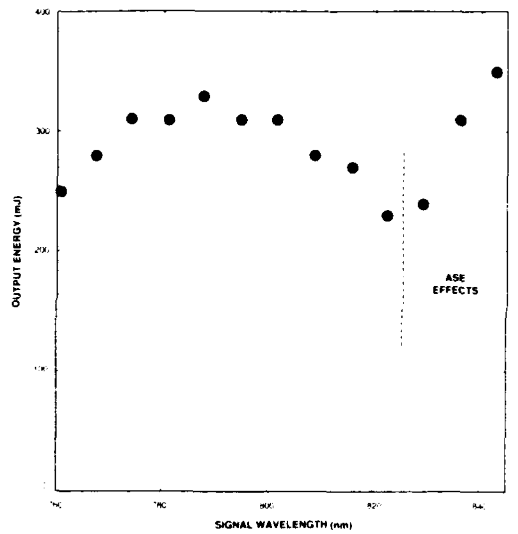

Fig. 11. The Ti:Al_2O_3 MOPA output energy per pulse as a function of wavelength. From 760 to 825 nm the energy per pulse varies by ~33%. For signal wavelengths greater than 825 nm, the output energy of the Ti:Al_2O_3 MOPA increases with increasing wavelength rather than decrease as would be expected from the gain profile of Ti:Al_2O_3. This increase is due to the onset of ASE which begins to contribute to the total output power of the Ti:Al_2O_3 MOPA.

Temporal and Spectral Characteristics

The shot to shot variation of the Ti:Al_2O_3 MOPA output is shown for fifteen consecutive pulses in Fig. 10. The pulses have been overlapped for ease of comparison and the pulsewidth of an individual pulse is ~115 ns FWHM. Amplitude variations are < 10% and the temporal jitter is ~20 ns with respect to the *Q*-switch trigger of the Nd:YAG MOPA. The temporal jitter is about the same as the jitter of the Nd:YAG MOPA macropulses. The pulses are smooth and show no structure on times as small as 20 ns as long as ASE is small. The amplitude variations of the Ti:Al_2O_3 output are comparable to the amplitude variations of our pump lasers which is to be expected since we are saturating the gain in the last amplifier stage.

The Ti:Al_2O_3 MOPA was tuned using a mechanical, three-plate, birefringent filter in the master oscillator leaving all other parameters unchanged. The output energy as a function of wavelength is shown in Fig. 11 where the data show that the system is broadly tunable from 760 to 825 nm. Over this range the energy per pulse varies by ~33%. The tuning range is limited on the short wavelength side by the reflectivity of the mirrors used in the Ti:Al_2O_3 MOPA.

On the long wavelength side, ASE limits the tuning range of the Ti : Al_2O_3 MOPA. ASE becomes evident when the master oscillator is tuned to a wavelength off the peak (~800 nm) of the gain profile where both the output of the master oscillator and the gain of the Ti : Al_2O_3 amplifier system decrease. ASE was measured using a spectrometer with a linear photodiode array at the exit aperture as a detector. This allowed us to simultaneously monitor the intensity from 760 to 820 nm. The spectrum showed a single narrow peak when no ASE was present. When ASE occurred the spectrum showed a broad "spiky" feature centered at the peak of the gain profile.

Fig. 11 shows that for signal wavelengths greater than 825 nm the output energy of the Ti : Al_2O_3 MOPA increases with increasing wavelength rather than decrease as would be expected from the gain profile of Ti : Al_2O_3. This increase is due to the onset of ASE which begins to contribute to the total output power of the Ti : Al_2O_3 MOPA. Spectra taken at wavelengths greater than 825 nm confirm this. Limitations on the tuning range due to ASE can be reduced by spatial or spectral filtering.

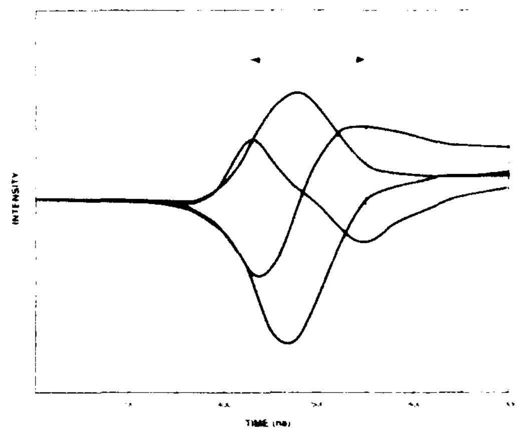

Fig. 12. Coherence of the Ti : Al_2O_3 MOPA. A sample of the master oscillator signal beam and the Ti : Al_2O_3 MOPA output beam were combined to generate an interference pattern. The intensity as a function of time for this beat signal was measured for a series of output pulses. One data set (for which the initial phase of the interferometer was fortuitous) exhibits a phase shift of $\sim\pi$ (indicated by the dashed vertical lines) occurring in a time on the order of 270 ns; this yields a frequency shift of 2 MHz.

Coherence

The coherence properties of the Ti : Al_2O_3 MOPA were investigated by interfering a sample of the master-oscillator output with a sample of the MOPA output. An uncoated wedge was positioned in the MOPA after the first isolator and before stage 1 to provide a sample of the master-oscillator beam. A second uncoated wedge provided a sample of the MOPA output beam and the two beams were combined with a mirror which transmitted 1% of the MOPA beam and reflected 99% of the Ti : Al_2O_3 master-oscillator beam. No attempt was made to stabilize the interferometer formed in this manner. Measurements of the interference pattern obtained by allowing a portion of the CW master-oscillator signal beam to be transmitted through the Ti : Al_2O_3 amplifier showed that fluctuations caused by environmental changes occurred on time scales much greater than 10 μs.

Typical signals (intensity versus time) detected with the interferometer described above are shown in Fig. 12 for a signal wavelength of 800 nm. When the Ti : Al_2O_3 MOPA was pumped, time dependent phase shifts were observed which are ascribed to both thermal and population-induced refractive index changes. The detected interferometer signal $I(t)$ can be modeled with the expression

$$I(t) = I_{MO} + I_{MOPA}(t) + 2\sqrt{I_{MO} I_{MOPA}(t)} \cdot \cos[\phi(t) + \phi_o] \quad (7)$$

where I_{MO} is the master-oscillator signal intensity, I_{MOPA} is the time dependent MOPA output intensity, $\phi(t)$ is the time dependent phase change that occurred when the MOPA was pumped, and ϕ_o is the initial random phase of the interferometer. One data set in Fig. 12 (for which the initial phase was fortuitous) exhibits a phase shift of $\sim\pi$ (indicated by the dashed vertical lines) occurring in a time on the order of 270 ns; this yields a frequency shift of 2 MHz. The intensity variation of the interferometer signal was consistent with (7) indicating that the output of the MOPA was completely coherent which together with the pulse width measurements imply a Fourier transform-limited bandwidth of ~4 MHz.

Conclusion

In summary, we have designed and constructed a Ti : Al_2O_3 master-oscillator/power-amplifier system. Pulse energies of up to 380 mJ at 800 nm were obtained. In the near field, the output beam of the Ti : Al_2O_3 MOPA is an elliptical Gaussian. The far field beam profile was also found to be an elliptical Gaussian and was measured to be ~1.1 × diffraction limited. We obtained 115 ns FWHM pulses which had ~10% pulse-to-pulse amplitude variations. The MOPA was tuned from 760 to 825 and the energy per pulse remained relatively constant. ASE is an issue for wavelengths greater than 825 nm. The coherence properties were tested and we observed a small frequency shift of 2 MHz due to both thermal and population induced index of refraction changes. The Fourier transform-limited bandwidth was inferred to be ~4 MHz.

Acknowledgment

The authors gratefully acknowledge V. Daneu, A. Walther, and R. Tapper for their contributions and many useful discussions. We would also like to thank R. E. Fahey and A. J. Strauss for growing most of the Ti : Al_2O_3 crystals used in this paper. The contributions of J. Weston and R. Ettelbrick (of Continuum) to the construction of the Nd : YAG MOPA are also gratefully acknowledged. We are grateful to M. Geis, K. Krohn, and B. J. Felton, for providing us with the random binary-phase plates. Finally, we would like to acknowledge M. D. Sciacca, L. Belanger, G. Lavoie, and H. C. Tran for their assistance.

References

[1] N. P. Barnes and D. K. Remelius, "Amplifier and line-narrowed oscillator performance of Ti : Al_2O_3," in *Tunable Solid-State Lasers II*, A. B. Budgor, L. Esterowitz, and L. G. DeShazer, Ed. New York: Springer-Verlag, 1986, pp. 218-227.

[2] K. F. Wall, R. L. Aggarwal, R. E. Fahey, and A. J. Strauss, "Small-signal gain in a Ti : Al_2O_3 amplifier," *IEEE J. Quantum Electron.*, vol. 24, pp. 1016-1020, 1988.

[3] L. G. DeShazer, J. M. Eggleston, and K. W. Kangas, "Oscillator and amplifier performance of Ti : sapphire," in *Tunable Solid-State Lasers II*, A. B. Budgor, L. Esterowitz, and L. G. DeShazer, Eds. New York: Springer-Verlag, 1986, pp. 228-234.

[4] F. Estable, F. Salin, M. Allain, P. Georges, and A. Brun, "Direct measurement of saturation fluence in Ti : Al_2O_3," *Opt. Commun.*, vol. 72, pp. 235-238, 1989.

[5] J. C. Barnes, N. P. Barnes, and G. E. Miller, "Master-oscillator power amplifier performance of Ti : Al_2O_3," *IEEE J. Quantum Electron.*, vol. 24, pp. 1029-1038, 1988.

[6] P. Georges, F. Estable, F. Salin, J. P. Poizat, P. Grangier, and A. Brun, "High-efficiency multipass Ti : sapphire amplifiers for a continuous-wave single-mode laser," *Opt. Lett.*, vol. 16, pp. 144-146, 1991.

[7] F. Salin, C. Rouyer, J. Squier, S. Coe, and G. Mourou, "Amplification of 1 ps pulses at 1.053 μm in a Ti : Al_2O_3 regenerative amplifier," *Opt. Commun.*, vol. 84, pp. 67-69, 1991.

[8] P. Brockman, C. H. Bair, J. C. Barnes, R. V. Hess, and E. V. Browell, "Pulsed injection control of a titanium-doped sapphire laser," *Opt. Lett.*, vol. 11, pp. 712-714, 1986.

[9] C. H. Bair, P. Brockman, R. V. Hess, and E. Modlin, "Demonstration of frequency control and CW diode laser injection control of a titanium-doped sapphire ring laser with no internal optical elements," *IEEE J. Quantum Electron.*, vol. 24, pp. 1045-1048, 1988.

[10] S. Basu, P. May, and J.-M. Halbout, "64-db amplification of 19-psec laser-diode pulses in a Ti-sapphire laser," *Opt. Lett.*, vol. 14, pp. 1272-1274, 1989.

[11] M. J. LaGasse, R. W. Schoenlein, J. G. Fujimoto, and P. A. Schulz, "Amplification of femtosecond pulses in Ti : Al_2O_3 using an injection seeded laser," *Opt. Lett.*, vol. 14, pp. 1347-1349, 1989.

[12] G. Rines and P. F. Moulton, "Performance of gain-switched Ti : Al_2O_3 unstable-resonator lasers," *Opt. Lett.*, vol. 15, pp. 434-436, 1990.

[13] A. J. W. Brown, C. H. Fisher, and D. D. Lowenthal, "Injection-seeded, narrow-band, flashlamp-pumped Ti : Al_2O_3 oscillator," in *Advanced Solid-State Laser*, H. P. Jensen and G. Dube, Eds. Wash. DC: OSA, 1991, pp. 94-100.

[14] T. D. Raymond and A. V. Smith, "Injection-seeded titanium-doped-sapphire laser," *Opt. Lett.*, vol. 16, pp. 33-35, 1991.

[15] A. Sullivan, H. Hamster, H. C. Kapteyn, S. Gordon, W. White, H. Nathel, R. J. Blair, and R. W. Falcone, "Multiterawatt, 100-fs laser," *Opt. Lett.*, vol. 16, pp. 1406-1408, 1991.

[16] P. A. Schulz, "Single-frequency ring laser," *IEEE J. Quantum Electron.*, vol. 24, pp. 1039-1044, 1988.

[17] K. W. Kangas, D. D. Lowenthal, and C. H. Muller III, "Single-longitudinal-mode, tunable, pulsed Ti : sapphire laser oscillator," *Opt. Lett.*, vol. 14, pp. 21-23, 1989.

[18] P. A. Schulz, "Wavelength independent Faraday isolator," *App. Opt.*, vol. 28, pp. 4458-4464, 1989.

[19] A. Walther, R. S. Tapper, and A. Sanchez, "Modeling for the design of high-gain-pulsed multistage laser amplifiers," in *Tech. Dig., CLEO 1988*, vol. 7. Wash. DC: OSA, 1988, p. 104.

[20] W. C. Scott and M. de Wit, "Birefringence compensation and TEM_{00} mode enhancement in a Nd : YAG laser," *Appl. Phys. Lett.*, vol. 18, pp. 3-4, 1971.

[21] P. Lacovara, K. F. Wall, R. L. Aggarwal, M. W. Geiss, and K. Krohn, "Laser pumping of solid state amplifiers using random binary phase plates," in *Advanced Solid State Lasers*, H. P. Jenssen and G. Dube, Eds. Wash., DC: OSA, 1991, pp. 106-107.

[22] Y. Kato, M. Mima, N. Miyanaga, S. Aringa, Y. Kitagawa, M. Nakatsuka, and C. Yamanaka, "Random phasing of high power lasers for uniform target acceleration and plasma instability suppression," *Phys. Rev. Lett.*, vol. 53, pp. 1057-1060, 1984.

[23] P. A. Schulz and S. R. Henmon, "Liquid nitrogen cooled Ti : Al_2O_3 laser," *IEEE J. Quantum Electron.*, vol. 27, pp. 1039-1047, 1991.

[24] K. F. Wall, R. L. Aggarwal, M. D. Sciacca, H. J. Zeiger, R. E. Fahey, and A. J. Strauss, "Optically induced nonresonant changes in the refractive index of Ti : Al_2O_3," *Opt. Lett.*, vol. 14, pp. 180-182, 1989.

K. F. Wall, photograph and biography not available at the time of publication.

Peter A. Schulz (M'91) was born in Boston, MA, in 1954. He received the B.S. degree from the Massachusetts Institute of Technology, Cambridge, and the Ph.D. degree from the University of California, Berkeley, both in physics. His dissertation focused on infrared multiphoton dissociation in a molecular beam.

While with the Joint Institute for Laboratory Astrophysics at the University of Colorado, he studied negative ions using threshold photodetachment spectroscopy. After joining the faculty of the Georgia Institute of Technology in 1982, he studied photodissociation and molecular beam kinetics using high-resolution vacuum ultraviolet and microwave spectroscopies. As a 1985 summer Fellow at Oak Ridge National Laboratory, he studied electron-impact ionization of multiply charged ions and electron-impact dissociation of H_2O^+. Since 1986 he has been at MIT Lincoln Laboratory, where he has developed Ti : Al_2O_3 lasers, frequency-modulated Nd : YAG lasers, and dispersion-compensated Faraday isolators. His current research interests are laser dynamics, novel lasers, and electrooptics.

Dr. Schulz is a member of the Optical Society of America.

R. L. Aggarwal, photograph and biography not available at the time of publication.

P. Lacovara, photograph and biography not available at the time of publication.

A. Sanchez, photograph and biography not available at the time of publication.